Structural evolution and giant magnetoresistance in electrodeposited Co-Cu/Cu multilayers

P. Chowdhury,[1] S. K. Ghosh,[2] Anjana Dogra,[1] G. K. Dey,[3] Yashwant G. Gowda,[1] S. K. Gupta,[1,*] G. Ravikumar,[1] A. K. Grover,[2] and A. K. Suri[4]

[1]*Technical Physics and Prototype Engineering Division, Bhabha Atomic Research Centre, Mumbai-400085, India*

[2]*Materials Processing Division, Bhabha Atomic Research Centre, Mumbai-400 085, India*

[3]*Materials Science Division, Bhabha Atomic Research Centre, Mumbai-400 085, India*

[4]*Materials Group, Bhabha Atomic Research Centre, Mumbai-400 085, India*

(Received 16 July 2007; revised manuscript received 26 March 2008; published 25 April 2008)

Structural transformations and their effect on giant magnetoresistance (GMR) were investigated in electrodeposited Co/Cu multilayers with varying Co-layer thicknesses (t_{Co}) in the range of 0.2–10 nm while keeping the Cu layer thickness (t_{Cu}) fixed at 4 nm. X-ray diffraction, scanning electron microscopy, cross-sectional transmission electron microscopy, and magnetization measurements were carried out to probe the structural transition from granular to semicontinuous to continuous Co layers. An unexpected result of the study is the observation of variations in GMR characteristics with a sharp peak in GMR at t_{Co}=0.5 nm followed by a broad peak at t_{Co}=3 nm. The GMR results have been analyzed in terms of ferromagnetic and superparamagnetic components for samples with varying t_{Co} to understand the structural evolution of the magnetoresistance behavior.

DOI: 10.1103/PhysRevB.77.134441 PACS number(s): 75.47.De, 75.70.−i, 75.30.Cr

I. INTRODUCTION

The developments in electrochemical science and technology for the past one and a half decades make it possible to synthesize high quality metallic multilayers with a layer thickness of 1 nm or less.[1,2] Multilayers of magnetic and nonmagnetic (NM) metals exhibit the giant magnetoresistance (GMR) effect, which is of interest for both scientific understanding and technological developments. In many of the studies reported in literature, the effect of the thickness of a nonmagnetic layer on GMR characteristics was mainly investigated. However, the studies on the effect of thickness of a ferromagnetic (FM) layer on the microstructure and GMR characteristics are equally important.

Among various multilayer systems showing GMR, Co/Cu multilayers have been quite extensively studied in the past few years.[3–16] Besides Co/Cu multilayers, granular Co-Cu alloys[17,18] and granular multilayers[3,19] also exhibit GMR. Granular multilayers that consist of a layer of grains of ferromagnetic materials separated by layers of nonmagnetic metal are a border between granular alloys and multilayers. Granular alloys are sometimes preferred due to their fully isotropic magnetoresistance (MR) behavior, negligible hysteresis, and low cost of preparation. However, due to a higher fraction of superparamagnetic (SPM) grains, high magnetic fields (~10 kG) are required to align the magnetic moments in granular alloys and, therefore, they display low magnetic field sensitivity. For magnetic sensor applications, the magnetic multilayers with improved field sensitivity, minimum hysteresis, and isotropicity in MR behavior are highly desirable.

Several investigations have been carried out to tailor the structure and morphology of the fragmented multilayer structure (in multilayer deposition) by controlling the free energy of surfaces and interfaces of magnetic and nonmagnetic phases.[19–23] By choosing a magnetic element with a high surface free energy[19] and with low miscibility of magnetic and nonmagnetic components, it has been possible to make magnetic clusters embedded in nonmagnetic regions when the thickness of magnetic layers is less than a few nanometers. This often leads to a heterogeneous mixture of FM and SPM[23] regions in a nonmagnetic matrix. A maximum GMR of 15% at 13 kOe was achieved in Co/Ag fragmented multilayers[20] prepared by sputtering.

Electrochemical deposition (ECD), among various deposition techniques, is an attractive alternative technique because of its simplicity, cost effectiveness, and high deposition rates in comparison to vacuum techniques. This technique is preferred in low-end applications such as GMR position sensors in automotive electronics or in microsystems.[24,25] A simple two-pulse plating approach utilizing a single solution electrolyte is usually employed to deposit Co-Cu/Cu multilayers (electrochemically deposited Co layers consist of a small fraction of Cu and are referred to as Co-Cu layers). However, electrochemically deposited multilayers usually show a lower GMR than those prepared by physical vapor deposition techniques and, therefore, there is a need for further investigations.

Considerable literature is available on the deposition of metallic multilayers by the ECD process.[4,22,26,27] Magnetic and magnetotransport properties were investigated in Co/Cu films with varying (both magnetic and nonmagnetic) layer thicknesses[3,4,28,29] and efforts were made to explain the experimentally observed GMR value by summing up the FM and SPM contributions.[22,30,31] Bakonyi *et al.*[22] explained the field dependence of MR as contributions from FM-FM, FM-SPM, and SPM-SPM scattering. The FM-FM scattering saturates at a field of 1.7 kOe, and the SPM contribution at larger fields is in agreement with the predictions of Wiser and co-workers.[32,33] Shima *et al.*[26] obtained a sigmoidal shape of the magnetization curve for a Co layer with a thickness (t_{Co}) less than 1.7 monolayers (ML). Their study did not show MR for $t_{Co}<1.7$ ML. For $t_{Co}>3.7$ ML, they observed in-plane fourfold symmetry with a dominance of magnetocrystalline anisotropy with increasing t_{Co}. Moreover, the understanding

of structural evolution with varying t_{Co} in Cu/Co multilayers deposited by ECD process is not satisfactory.

Recently, we reported[27] the results of magnetic and magnetotransport measurements on electrodeposited Co/Cu granular multilayers prepared under conditions in which practically no Co dissolution occurs and the multilayer structure was found to consist of FM and SPM nanoclusters separated by NM regions for samples with $t_{Co} < 1$ nm. Based on the model of Wiser and co-workers,[32,33] with the presence of FM and SPM particles, it has been shown that there are three possible routes of scattering mechanism, i.e., FM-FM, FM-SPM, and SPM-SPM, which lead to a large GMR value. At the critical thickness of $t_{Co}=0.5$ nm, the granular multilayer structure shows a large GMR of 8% with $H_c \sim 70$ Oe and a sensitivity of $\sim 0.03\%/\text{Oe}$. In the present study, we have focused our attention on understanding the structural as well as the associated magnetic and/or magnetoresistance property evolutions with the increase in t_{Co}.

In the present study, we have synthesized Co/Cu multilayers by pulse electrodeposition with varying t_{Co} (from 0.2 to 10 nm) while keeping the Cu layer thickness fixed ($t_{Cu}=4$ nm). The structural transformation from continuous multilayers for large t_{Co} to granular multilayers (at lower t_{Co}) has been investigated by x-ray diffraction (XRD), scanning electron microscopy (SEM), and cross-sectional transmission electron microscopy (XTEM). The influence of structural transition on both magnetization and magnetoresistance has also been discussed. An interesting result of the study is the variations in magnetoresistance that are measured as a function of t_{Co}.

II. EXPERIMENT

Co-Cu/Cu multilayers were electrochemically deposited on Si(111)/Ti(20 nm) substrates as described earlier.[27] Briefly, a thin film buffer layer of Ti (20 nm thick) and a seed layer of Cu (20 nm thick) were deposited at room temperature on (111) oriented silicon substrates by rf sputtering. Before the deposition of a multilayer, a copper seed layer was acid cleaned for 10 s to remove the oxide layer formed over it. A single sulfate based electrolyte that contained $Co^{+2}:Cu^{+2} \approx 250:1$ and had a *p*H of 2.7 were used for electrodeposition at 298 ± 1 K. The solutions were freshly prepared by using analytical grade reagents and de-ionized water (resistivity of 18 $M\Omega$ cm) from a Millipore Milli-Q water purification system. A Pt foil was used as a counter-electrode. Multilayers were potentiostatically grown by using a two-pulse method in a three-electrode cell while keeping the total charge constant in alternate pulses. The typical potential pulses applied for Co and Cu were −1.4 and −0.6 V, respectively, with respect to a standard saturated calomel electrode. Initial experiments were carried out with varying t_{Cu} while keeping t_{Co} constant to determine optimum t_{Cu} for maximum MR. The thickness of the films was optimized by using an electrochemical quartz crystal microbalance.[28] To investigate the effect of t_{Co}, $[\text{Co}(t_{Co})/\text{Cu}(4\ \text{nm})]_{50}$ multilayers with varying t_{Co} and fixed t_{Cu} of 4 nm (optimum value) were grown. Prepared multilayers with Co-layer thicknesses of t_{Co}=0.2, 0.3, 0.4, 0.5, 0.6, 0.7, 0.8, 1.0, 2.0, 3.0, 5.0, 7.0, 8.0, and 10 nm are designated as S2, S3, S4, S5, S6, S7, S8, S10, S20, S30, S50, S70, S80, and S100, respectively.

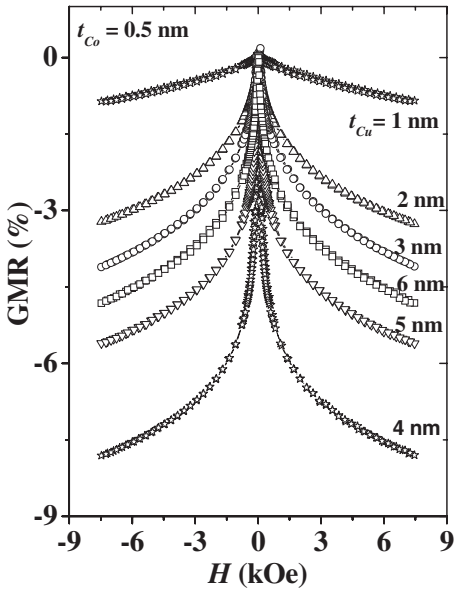

FIG. 1. GMR characteristics as function of applied magnetic field for Co/Cu multilayers with different Cu-layer thicknesses (t_{Cu}) and constant t_{Co}=0.5 nm.

XRD spectra of these multilayers were acquired on a Philips X'pert diffractometer (using Cu $K\alpha$ radiation). The surface morphology of Co/Cu multilayers was investigated by using TESCAN Vega-MV 2300T-40 SEM. The XTEM studies were carried out by using a JEOL-2000FX electron microscope to reveal the layer structure. Magnetization measurements with respect to field and temperature were performed by using a superconducting quantum interference device magnetometer. MR measurements for all of the samples were carried out at room temperature by using a four-probe method in a strip geometry and by using applied magnetic fields in the range from −7.5 to +7.5 kOe. The magnetic field (H) was kept in the plane of the film but perpendicular to the applied current (I) direction for the measurement of transverse MR (TMR). For the longitudinal MR (LMR) component, the applied field direction was kept along the current direction. Magnetoresistance in this paper is defined as $\text{MR}=\Delta R/R=(R_H-R_{\text{Max}})/R_{\text{Max}}$, where R_H is the resistance measured in a magnetic field H and R_{Max} is the maximum resistance measured as a function of field. Both LMR and TMR components are largely negative and the measured anisotropic magnetoresistance (AMR)=LMR −TMR was found to be within 1% for most of the samples and, for simplicity, we have considered only the TMR data for discussion.

III. RESULTS AND DISCUSSION

A. Effect of Cu layer thickness

The dependence of MR on the spacer layer thickness, t_{Cu}, for multilayers, $[\text{Co}(0.5\ \text{nm})/\text{Cu}(t_{Cu})]_{50}$, with fixed t_{Co} is shown in Fig. 1. It is seen that the MR initially increases with thickness and attains its maximum value for t_{Cu} of 4 nm

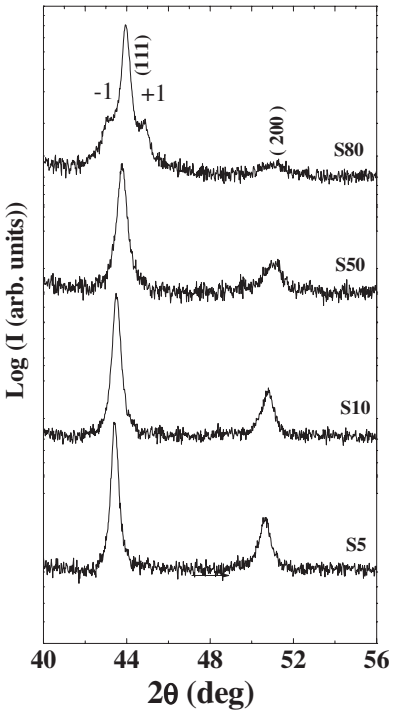

FIG. 2. XRD pattern for Co/Cu multilayer samples with the Co-layer thickness varying between 0.5 nm (S5) and 8 nm (S80).

and decreases for higher thicknesses. A continuous decrease in MR with t_{Cu} above 4 nm is in agreement with earlier results,[34] and the magnitude of the MR effect in our electrodeposited multilayers is comparable to sputter deposited or molecular beam epitaxy grown samples, which indicates that electrodeposition is a competitive method for obtaining high quality multilayers. The Co/Cu system is known to exhibit two peaks in MR, at $t_{Cu} \sim 1.5$ nm and ~ 3.5 nm.[10,11] The maximum in the present study for $t_{Cu}=4$ nm is in agreement with the second peak expected for this system. The reason for the nonobservance of the first peak is that we have made measurements at 1 nm intervals and the width of the first peak is less than 1 nm.

B. X-ray diffraction

The x-ray diffraction spectra of the multilayers with different Co layer thicknesses t_{Co} are shown in Fig. 2. The spectra shows a fcc lattice of both Cu and Co. It is seen that the films are predominantly oriented along the (111) direction and the degree of orientation improves with an increase in Co-layer thickness. It is seen that the position of the (111) peak shifts from 43.41° to 43.91° and the linewidth broadens as the Co layer thickness increases from 0.5 to 8 nm. We may note that the position of this peak is at 44.23° for pure Co and 43.31° for Cu.[35] The lattice parameters are close to that of Cu at small thicknesses and increase toward that of Co at larger t_{Co}. Therefore, the results indicate that (a) the Co layer is stressed, i.e., compressed for all films and the stress decreases as the t_{Co} increases, and (b) there is an increase in lattice parameter variation in the films at higher t_{Co} as indicated by the broadening of the peak. This variation is expected as Co layers at the interface with Cu would have a maximum stress, and the stress would be lower at Co layers away from the interface.

A multilayer structure is indicated by the observation of satellite peaks to main XRD peaks.[3,13] No clearly defined satellites were seen for multilayers with lower Co layer thicknesses, but for $t_{Co}=8$ nm, first order satellites peaks on both sides of the main peak were observed. The absence of clear satellites for small t_{Co} indicates that thinner films do not have smooth and continuous layers. As indicated by SEM studies (discussed later), this is due to the granular nature of Co layers with small t_{Co}. Their low intensity and the nonobservation of satellite peaks for smaller t_{Co} indicate a partly diffusive nature of interfaces. The bilayer period $\Lambda(=t_{Co}+t_{Cu})$ can be calculated by using the position $(\theta \pm n)$ of satellite peaks in the following equation:[36]

$$\frac{2 \sin \theta \pm n}{\lambda} = \frac{1}{d} \pm \frac{n}{\Lambda},$$

where d is the lattice spacing, n is the order of the satellite peak, and λ (1.5406 Å) is the wavelength of the x rays. The calculated bilayer period for $[\mathrm{Co}(8\ \mathrm{nm})/\mathrm{Cu}(4\ \mathrm{nm})]_{50}$ is 10.3 nm. Above results indicate that an increase in Co-layer thickness helps in making the superlattice structure coherent as well as improve the (111) orientation.

C. Scanning electron microscopy and cross-sectional transmission electron microscopy investigations

Surface morphology of as deposited multilayers with different t_{Co} was studied by SEM and the results are shown in Fig. 3. Films for larger t_{Co} (5 nm) have a smooth morphology that changes to a granular structure with a reduction in t_{Co}. The results are in agreement with XRD data (where satellite peaks were not observed for small t_{Co}) and indicate transformation from coherent multilayers to a granular multilayer structure with a reduction in t_{Co}. For small t_{Co}, Co layers may grow as islands with a poor coverage of the underlying Cu layers, which results in films that have a granular morphology. This observation corroborates the previous investigations regarding island growth of Co on Cu(111) surface for small t_{Co}.[37,38]

Figure 4 shows the cross-sectional transmission electron microscopy (TEM) of some multilayers. The results show a layered structure for sample S50 and a granular nature for sample S4 with a 0.4 nm Co-layer thickness. The layer pattern for S50 is wavy, which indicates diffuse multilayers. The results are in agreement with SEM and XRD data. The columnar growth of Co grains for smaller t_{Co} seen in Fig. 4(a) is also in agreement with the observations of Shima *et al.*[39]

D. Magnetization

M-H curves for multilayers with different Co layer thicknesses are shown in Fig. 5. Magnetization as a function of temperature under field-cooled and zero-field-cooled conditions for samples S2, S3, and S8 are shown in the insets of Fig. 5. The dependence of coercivity (H_c) and remnant magnetization (M_r) on Co-layer thickness obtained from the data

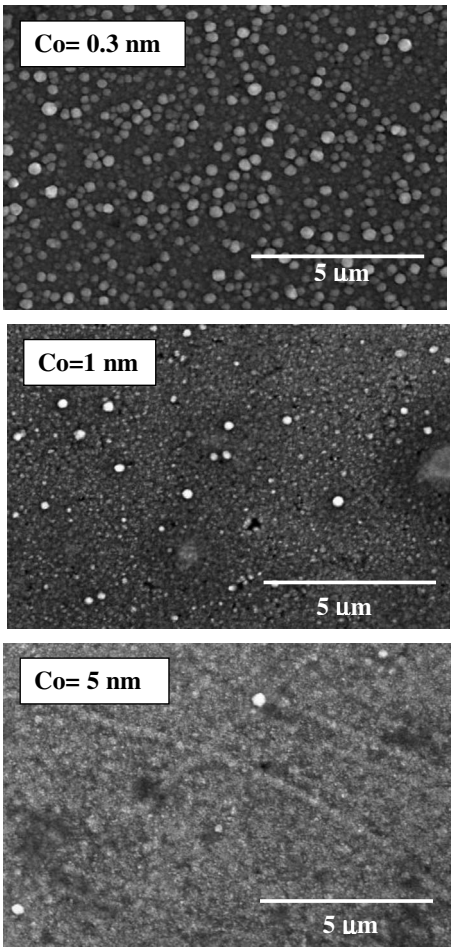

FIG. 3. SEM micrographs of multilayers with Co-layer thicknesses of 0.3 nm (S3), 1.0 nm (S10), and 5 nm (S50).

in Fig. 5 are shown in Fig. 6 and the following observations are made:

(a) Hysteresis starts appearing for the samples with thicknesses $t_{Co} > 0.4$ nm. The coercive field H_c measured

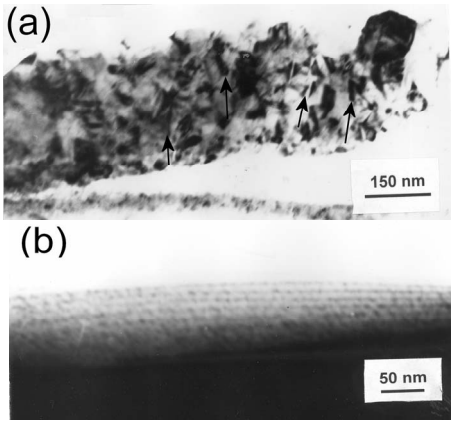

FIG. 4. XTEM micrographs of multilayer samples (a) S4 and (b) S50. The dark band in the lower side of the figure in (b) is due to the unthinned portion of the sample and the Si substrate with 20 nm Ti buffer and 20 nm Cu seed layer.

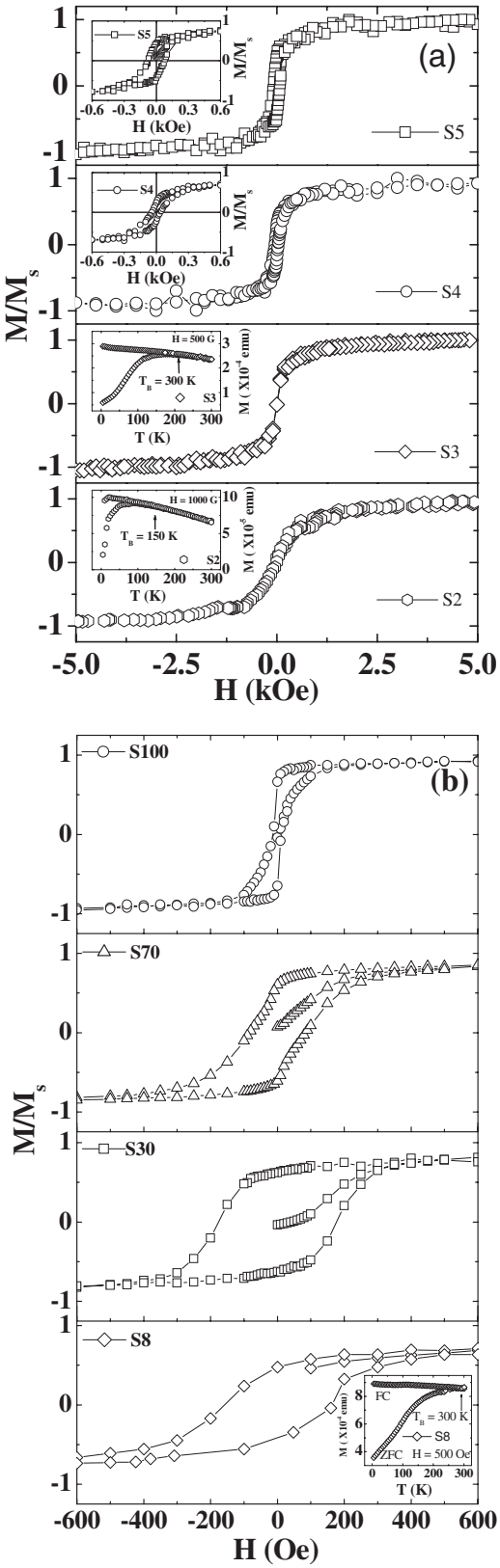

FIG. 5. [(a) and (b)] Room temperature $M(H)$ hysteresis curves for samples with different Co-layer thicknesses. The insets for samples S2, S3, and S8 show a temperature variation of magnetization under field-cooled and zero-field-cooled conditions. The insets for samples S4 and S5 show magnified $M(H)$ curves.

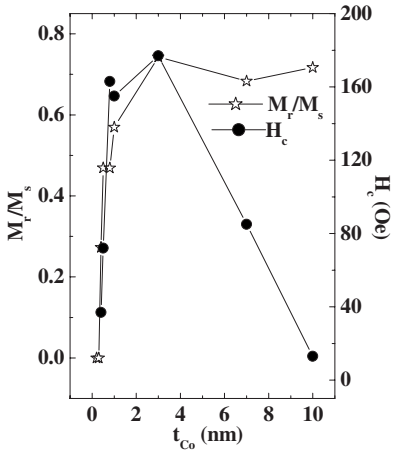

FIG. 6. Remnant in-plane magnetization M_r and coercivity H_c plotted as a function of the t_{Co}. Here, M_r has been plotted as the ratio M_r/M_s, wherein M_s is the saturation magnetization.

from these hysteresis curves show that it sharply increases with t_{Co}, attains a maximum for t_{Co} in the 2–4 nm range, and then gradually decreases at higher thicknesses.

(b) A comparison of field-cooled and zero-field-cooled data shows that the blocking temperature T_B increases with t_{Co}, from 150 K for S2 (t_{Co}=0.2 nm) to 300 K for S8 (t_{Co}=0.8 nm).

(c) M_r increases with t_{Co} and saturates at large t_{Co}.

Based on these observations, we will try to correlate them with the microstructure of the multilayers.

The absence of hysteresis (M_r=0 and H_c=0) and the sigmoidal shape of the magnetization curve indicate that samples with low Co thicknesses consist of superparamagnetic particles separated by Cu layers, and the details of the analysis were reported elsewhere.[27] The isotropic granular Langevin-type superparamagnetic system is further confirmed by low blocking temperatures of 150 and 200 K for samples S2 and S3, respectively. Hysteresis curves for films with higher t_{Co} indicate a gradual transition from granular multilayers consisting of superparamagnetic particles to layers with a combination of FM and SPM particles and, finally, to well defined ferromagnetic layers. A combination of ferromagnetic and SPM particles is indicated by the data of sample S4 with a small hysteresis and nonsaturation of magnetization with field. This transition is in accordance with the microstructure change from granular to layered films, as indicated by the TEM and XRD data.

The gradual transition from SPM particles to SPM/FM particles and ferromagnetic layers as discussed above explains the increase in coercive field H_c with t_{Co} in the 0–3 nm range. The reduction in coercivity for $t_{Co}>3$ nm is ascribed to the combined effect of the following mechanisms: (a) the reducing effect of domain wall pinning at the interface between Co and Cu layers as the film thickness increases[40] (domain wall pinning may also decrease due to a better planarity of films as the Co-layer thickness increases); (b) the reduction in compressive stress with increasing thickness, as shown by the XRD data discussed above (Cai *et al.*[41] observed a similar increase in coercivity due to a compressive stress in Co/MgO multilayers with a maximum coercivity at t_{Co}=3 nm as observed by us; they reported that the effect of the compressive stress may be maximum for the interface layer between Co and Cu layers); and (c) the effect of domain wall motion as was used by Néel[42] to obtain the well known relation $H_c=t^{-4/3}$, which describes the reduction in coercive field with thickness.

We now discuss the dependence of remnant magnetization M_r (plotted as M_r/M_s, where M_s is the saturation magnetization) on t_{Co} as shown in Fig. 6. It is observed that M_r increases with t_{Co} and saturates at $t_{Co}\sim 3$ nm. The increase in M_r with t_{Co} is attributed to a gradual transition from SPM Co particles to FM particles and layers. The saturation in M_r at 3 nm is also in agreement with the thickness variation of H_c and confirms that an increase in H_c with $0<t_{Co}<3$ nm is due to a reduction in SPM particle density, and once most of the SPM particles have converted to FM layers, H_c starts decreasing due to a combination of the mechanisms listed above.

E. Magnetoresistance

The field dependence of MR for different samples is shown in Fig. 7 and the variation in GMR (at 7.5 kG) with t_{Co} is depicted in Fig. 8. A hysteresis in MR [Fig. 7(a) inset] is also observed for samples with larger t_{Co}. We note that a buffer layer of Ti (20 nm) and a seed layer of Cu (20 nm) provide a parallel path for current that does not contribute to MR. For a multilayer $[\mathrm{Co}(0.2\ \mathrm{nm})/\mathrm{Cu}(4\ \mathrm{nm})]_{50}$ with minimum t_{Co}, the combined thickness of buffer and seed layers is nearly 19% of the multilayer thickness. While this will reduce measured GMR (by a maximum of 19%), it will not influence the conclusions of the study as the sample to sample variation of error will be smaller and the error will monotonically vary with Co thickness. For further analysis, we have plotted in Fig. 8(b) the MR hysteresis measured as the peak field (H_p) of the magnetoresistance curves [see the inset of Fig. 7(a)] along with the coercive field H_c. From the data in Figs. 7 and 8, we can deduce the following conclusions:

(a) The value of GMR increases with t_{Co}, attains a sharp maximum at t_{Co}=0.5 nm, and then decreases to have a sharp minimum at 0.6 nm, followed by a broad maximum between 1 and 3 nm and decreases thereafter. This variation in GMR with t_{Co} is unexpected, while the magnetic coupling between layers (which depends on Cu layer thickness t_{Cu}) is normally a cause of a similar behavior.

(b) The hysteresis in MR measured by H_p in Fig. 8(b) is quite small for $t_{Co}<0.5$ nm and sharply increases for t_{Co}=0.6 nm, followed by a broad peak, and falls at larger thicknesses. The small random variation in the H_p data between 0.6 and 7 nm may be due to statistical variations and has not been considered. A closer look into the curves of Fig. 8(b) shows that the difference in resistance maximum (H_p) and coercivity (H_c) at lower t_{Co} (0.5 nm) is smaller as compared to higher t_{Co}. Basically, the maximum resistance state in MR arises when the neighboring layer magnetizations have the most disordered state within the spin diffusion length scale. On the other hand, the coercivity measures the

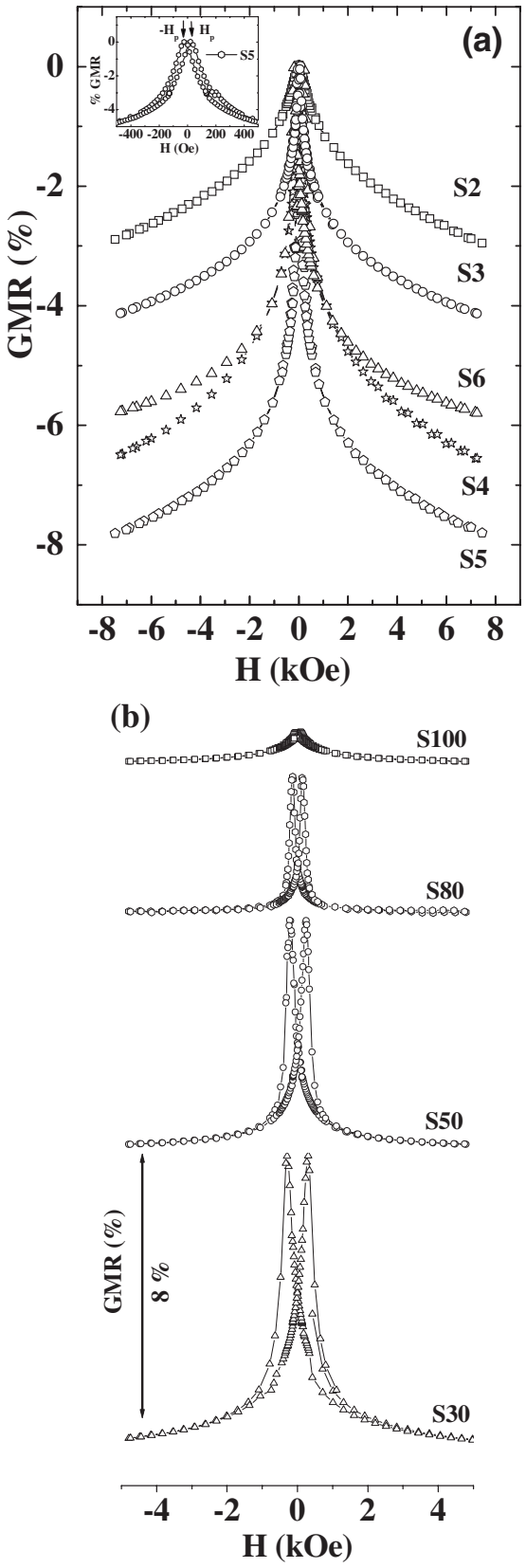

FIG. 7. [(a) and (b)] Field dependence of magnetoresistance for samples with different Co-layer thicknesses. The inset in (a) shows the GMR of sample S5 at low field with the definition of the MR peak field H_p.

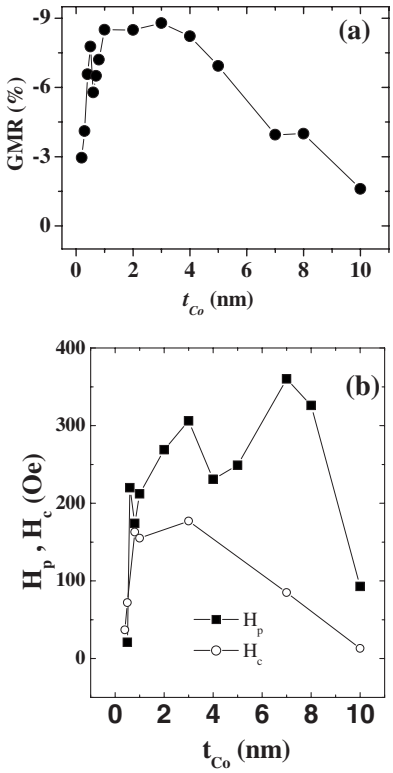

FIG. 8. (a) Magnetoresistance at the highest field used (7.5 kOe) in the study and (b) the peak field H_p and the coercive field H_c as a function of t_{Co}. Here, the peak field H_p is the peak value of the MR in the data in Fig. 7.

magnetic field where the overall magnetization has the most disordered state, which results in zero net magnetization. Obviously, the two kinds of disorder should not necessarily occur at the same magnetic field: they can be very different or they can be very close to each other depending on the relative spatial arrangement of the SPM and FM regions.[43] This twofold situation is clearly exemplified by our data in Fig. 8(b): H_c and H_p are close to each other for low t_{Co} values and H_p is much larger than H_c for high t_{Co} values. This finding is in good agreement with the results of Ref. 43. In both works, H_p is close to H_c when the SPM term dominates the total GMR, and H_p is larger than H_c when the FM term dominates. For dominating SPM regions, the overall and local random magnetic orientations can be expected to occur at the same magnetic field values, whereas for mostly FM regions, the occurrence of a maximum local magnetic disorder may require a larger external magnetic field than just the coercivity providing the condition for overall randomness only.

To understand these results, we have analyzed the field dependence of the magnetoresistance for all of the samples on the basis of the decomposition of FM and SPM contributions by using the method described by Bakonyi *et al.*[22] According to them, there are mainly two terms, $GMR_{FM\text{-}FM}$ and $GMR_{FM\text{-}SPM}$, which contribute to the total GMR. $GMR_{FM\text{-}FM}$ occurs due to spin dependent electron scattering phenomenon when the electron travels along the path "FM $\rightarrow$ NM $\rightarrow$ FM," whereas scattering along the electron path "FM $\rightarrow$ NM $\rightarrow$ SPM" gives rise to the $GMR_{FM\text{-}SPM}$ term. The

$GMR_{FM\text{-}SPM}$ field dependence of $MR(H) \propto L(x), L(x)$ is a Langevin function, where $x = \mu H / k_B T$. Here, μ is the magnetic moment of the SPM particle and k_B is the Boltzmann constant. An additional contribution from "SPM→NM →SPM" scattering, i.e., $(GMR_{SPM\text{-}SPM})$, can be considered as well, where the magnetoresistance dependence on the square of the Langevin function $[L(x)]$ was predicted: $MR(H) \propto \{L(x)\}^2$.[32,33] Therefore, the total GMR can be written as the sum of three contributions as follows: $GMR(H) = GMR_{FM\text{-}FM} + GMR_{FM\text{-}SPM} + GMR_{SPM\text{-}SPM}$. Previous experience[22,32,33,43] has shown, however, that in the case of a significant $GMR_{FM\text{-}SPM}$ contribution, the last term here, $(GMR_{SPM\text{-}SPM})$, is usually negligible and we shall also neglect it.

Moreover, an AMR contribution due to the FM regions is unanimous, and here, we take it into consideration by writing $MR(H) = GMR_{FM\text{-}FM} + AMR$, similar to the procedure in Ref. 22. Similar to the magnetization of the FM particles saturated at fields of $H_s \sim 1-2$ kOe, both $GMR_{FM\text{-}FM}$ and AMR contributions become independent of the magnetic field for $H > H_s$. In this situation, we can consider that MR arises from a current flowing along paths connected in series: path A (FM→NM→FM) gives rise to $GMR_{FM\text{-}FM}$, path B (starting and ending in a given large FM region) gives rise to AMR, with these two first terms dominating at low fields, and, finally, path C (FM→NM→SPM) gives rise to $GMR_{FM\text{-}SPM}$, which dominates at high fields. Therefore, for $H > H_s$, the field dependence of $MR(H)$ can be described as[22]

$$\begin{aligned} MR(H) &= GMR_{FM\text{-}FM} + AMR + GMR_{FM\text{-}SPM} L(x) \\ &= MR_{FM} + GMR_{FM\text{-}SPM} L(x). \end{aligned} \quad (1)$$

Typical results of the decomposition analysis for samples S3 and S50 are shown in Fig. 9. During this analysis, for $H > H_s = 2.0$ kOe, the $MR(H)$ data were fitted by using Eq. (1) and good agreement between the experimental data and Eq. (1) was observed. We have tried to fit the experimental $MR(H)$ data by also taking into account the $GMR_{SPM\text{-}SPM}$ term, but there was no improvement in the fit, which is in agreement with previous findings.[22,43] We note some interesting results, in which the decomposed GMR in S3 shows FM contributions even though the M-H curve indicates no FM moments. This could be due to the limitations of the measurement techniques in detecting the lower volume fraction of FM regions. It was also seen that the $GMR_{FM\text{-}FM}$ contributions increased with the increase in t_{Co} with the loss of $GMR_{FM\text{-}SPM}$.

The variation in total magnetoresistance and its decomposed FM-FM and FM-SPM contributions as a function Co-layer thickness are plotted in Fig. 10(a), and the SPM cluster size inferred from $MR(H)$ fitted data is shown in Fig. 10(b). As shown in Fig. 10(a), the SPM contribution in total GMR initially increases for $t_{Co} < 0.5$ nm and then it starts decreasing with t_{Co}. At $t_{Co} \sim 3$ nm onward, the SPM moment is found to quite rapidly decay and becomes negligible for $t_{Co} \sim 8$ nm. On the other hand, FM contribution to GMR rapidly increases up to $t_{Co} = 3$ nm and then decreases further with t_{Co}. As shown in Fig. 10(b), the increase in SPM magnetic moment with t_{Co} up to 3 nm and the subsequent decay

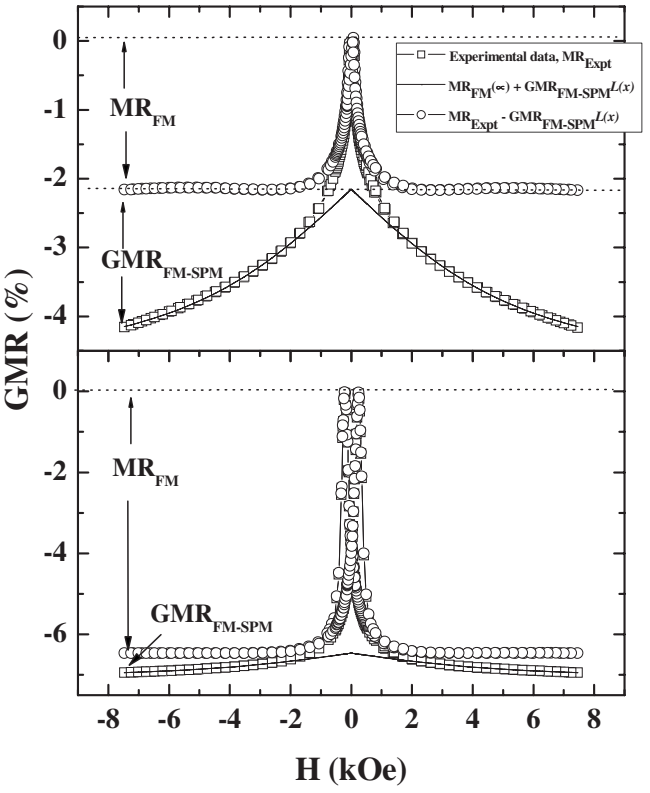

FIG. 9. Results of decomposed $GMR_{FM\text{-}FM}$ and $GMR_{FM\text{-}SPM}$ contributions for samples S3 and S50. The experimental $MR(H)$ data for $H > 2.0$ kOe are fitted by using Eq. (1), which yields the $GMR_{FM\text{-}SPM}$ term. The $GMR_{FM\text{-}FM}$ is obtained by subtracting the $GMR_{FM\text{-}SPM}$ term from the experimental data in the measured field range.

imply the lateral growth of isolated islands in the magnetic layer plane, which are magnetically decoupled from the FM part of the magnetic layers. This observation suggests that the isolated SPM and FM regions laterally grow with enhanced moment at the expense of smaller SPM regions. The morphology of the isolated SPM regions could be spherical at the beginning because of the immiscibility of Co in Cu. As t_{Co} increases, the morphology changes to ellipsoidal to rhomboidal because of coalescence of neighboring Co grains along the plane of the layer. This understanding of morphological growth within a Co layer explains the columnar structure obtained at lower t_{Co} from XTEM investigations. By considering $\mu_{Co} = 1.7$ μ_B/atom and 5 at. % Cu within the magnetic layer, we obtain an island size of 920 atoms for $t_{Co} = 0.2$ nm and an island size of 1900 Co atoms for $t_{Co} = 3.0$ nm, which further corroborates the above growth process from an individual island to a discontinuous layer to a continuous layer. Beyond $t_{Co} \sim 3$ nm, the gradual decrease in SPM moment indicates a depletion of isolated SPM regions and a retention of unaccommodated SPM regions lying within the valley regions of previously deposited rough Cu layer (Cu-Co interface regions). The same is true for the upper surface of the growing Co layer (Co-Cu interface). Moreover, at higher thicknesses, the planarity of the Co layer also increases due to the occurrence of miscibility within the same element, which allows the growth front of FM regions

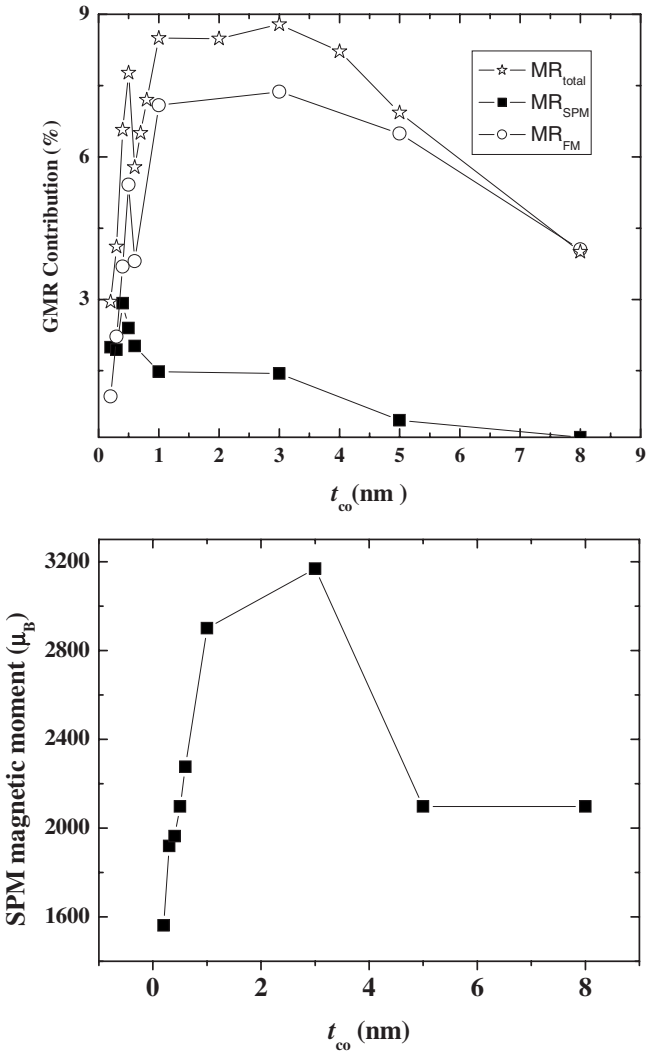

FIG. 10. (a) The variation in the total MR and its decomposed FM-FM and FM-SPM contributions are shown as a function of the Co-layer thickness. (b) The SPM cluster size inferred from the fitted MR(H) data is shown.

to accommodate most of the SPM regions, retaining a few within the interface roughness. Therefore, it is natural that the probability of the FM-FM scattering event will increase at the cost of SPM-SPM interactions at reasonably higher t_{Co}, which corroborates our earlier GMR analytical results.[27]

Similarly, for better understanding of the GMR variations below $t_{Co}<1$ nm, the interlayer and intralayer scattering[44] phenomena have been considered. The hysteresis in GMR [Figs. 7 and 8(b)] and magnetization hysteresis curves indicate that the films transform from predominantly granular SPM particle based multilayers to multilayers with nearly homogeneous Co layers, with FM characteristics over the 0.5–1 nm range of t_{Co}. For $t_{Co}<0.5$ nm, the grains are separate from each other and the intralayer FM-FM and FM-SPM scattering (i.e., between grains within a layer) predominate. This leads to increasing MR in the 0–0.5 nm range as (i) the grain size increases, which leads to a better magnetization of grains, and (b) the distance between grains decreases (due to the larger size and number of grains) to less than the spin diffusion length. A distance less than the spin diffusion length is necessary to observe GMR that is caused by spin dependent scattering between grains.[43] As shown by the sharp increase in hysteresis in MR in Fig. 8(b), and in the magnetization in Fig. 6, a gradual transition from predominantly granular films to layered structures with FM properties occurs at $t_{Co}\sim 0.6$ nm. Due to the formation of a layered structure, intragrain scattering (i.e., scattering between Co grains within a layer) is suddenly reduced. This leads to a sharp reduction in maximum GMR at $t_{Co}=0.6$ nm. However, the calculated SPM moment [Fig. 10(b)] is found to gradually increase from 0 to 1 nm with t_{Co} because of the increased size of the SPM grains. So, basically the drop in MR at $t_{Co}\sim 0.6$ nm depends on the morphology of magnetic regions, their distribution, and interparticle separation. For $1>t_{Co}>0.6$ nm, the layered structure improves and GMR increases due to an increase in scattering between layers, with some degree of antiparallel alignment in the absence of field and parallel alignment upon application of field. Finally, at $t_{Co}=3$ nm, as shown by the M_r and H_c data, there are almost no separate grains left and intralayer scattering (between SPM or FM grains) completely disappears. For higher t_{Co}, the GMR decreases, as many electrons scatter within a ferromagnetic Co layer both in the absence or in the presence of a magnetic field and do not contribute to GMR.

IV. CONCLUSION

The effect of Co-layer thickness at a fixed Cu-layer thickness in electrochemically deposited Co-Cu/Cu multilayers was found to show variations in GMR characteristics with peaks in GMR at 0.5 and 3.0 nm. The results have been understood in terms of a gradual morphological transition of the Co layer from a granular to a continuous layer pattern as the Co-layer thickness increases. Both the magnetization and the MR measurements mapped the changes in the magnetic structure of the samples from SPM dominant granules to discontinuous FM-SPM mixtures to a FM dominant continuous layer with the increase in Co-layer thickness. The decomposition of total GMR showed two major contributions, i.e., $GMR_{FM\text{-}FM}$ and $GMR_{FM\text{-}SPM}$, and led to the conclusions that with an increase in t_{Co}, the percentage of FM contribution increases at the expense of the SPM regions. The difference in H_p and H_c was also found to increase with the increase in t_{Co}.

*Corresponding author. drgupta@barc.gov.in

[1] C. A. Ross, Annu. Rev. Mater. Sci. **24**, 159 (1994).
[2] W. Schwarzacher and D. S. Lashmore, IEEE Trans. Magn. **32**, 3133 (1996).
[3] L. Péter, A. Cziŕaki, L. Pogény, I. B. Z. Kupay, M. Uhlemann, M. Herrich, T. B. B. Arnold, and K. Wetzig, J. Electrochem. Soc. **148**, C168 (2001).
[4] V. Weihnacht, L. Péter, J. Tóth, J. Pádàr, Z. Kerner, C. M. Schneider, and I. Bakonyi, J. Electrochem. Soc. **150**, C507 (2003).
[5] S. Z. Hua, D. S. Lashmore, L. J. Schwarzendruber, J. W. Egelhoff, K. Raj, and H. D. Chopra, J. Appl. Phys. **81**, 4582 (1997).
[6] E. A. M. van Alphen, A. H. J. Colaris, S. K. J. Lenczowski, C. Schonenberger, M. A. M. Gijs, and W. J. M. de Jonge, J. Magn. Magn. Mater. **156**, 29 (1996).
[7] P. Nallet, E. Chassaing, M. G. Walls, and M. J. Hytch, J. Appl. Phys. **79**, 6884 (1996).
[8] E. Chassaing, A. Morrone, and J. E. Schmidt, J. Electrochem. Soc. **146**, 1794 (1999).
[9] Y. Jyoko, S. Kashiwabara, and Y. Hayashi, J. Electrochem. Soc. **144**, L5 (1997).
[10] Y. Ueda, N. Hataya, and H. Zaman, J. Magn. Magn. Mater. **156**, 350 (1996).
[11] Y. Ueda, N. Kikuchi, S. Ikeda, and T. Houga, J. Magn. Magn. Mater. **198-199**, 740 (1999).
[12] M. Shima, L. Salamanca-Riba, T. P. Moffat, R. D. McMichael, and L. J. Schwarzendruber, J. Appl. Phys. **84**, 1504 (1998).
[13] M. Shima, L. Salamanca-Riba, T. P. Moffat, and R. D. McMichael, J. Magn. Magn. Mater. **198-199**, 52 (1999).
[14] M. Shima, L. Salamanca-Riba, and T. P. Moffat, Electrochem. Solid-State Lett. **2**, 271 (1999).
[15] K. Attenborough, H. Boere, J. D. Boeck, G. Borghs, and J. Celis, Appl. Phys. Lett. **74**, 2206 (1999).
[16] P. E. Bradley and D. Landolt, Electrochim. Acta **45**, 1077 (1999).
[17] J. Q. Xiao, J. S. Jiang, and C. L. Chien, Phys. Rev. Lett. **68**, 3749 (1992).
[18] E. Gómez, A. Labarata, A. Llorente, and E. Valls, J. Electrochem. Soc. **151**, C731 (2004).
[19] F. Spizzo, E. Angeli, D. Bisero, P. Vavassori, and F. Ronconi, Appl. Phys. Lett. **79**, 3293 (2001).
[20] E. A. M. van Alphen and W. J. M. de Jonge, Phys. Rev. B **51**, 8182 (1995).
[21] D. J. Kubinski and H. Holloway, J. Magn. Magn. Mater. **165**, 104 (1997).
[22] I. Bakonyi, L. Péter, Z. Rolik, K. Kiss-Szabó, Z. Kupay, J. Tóth, L. F. Kiss, and J. Pádár, Phys. Rev. B **70**, 054427 (2004).
[23] S. Paje, M. Arranz, J. Andres, and J. Riverio, J. Phys.: Condens. Matter **15**, 1071 (2003).
[24] J. M. Daughton, J. Magn. Magn. Mater. **192**, 334 (1999).
[25] C. P. O. Treutler, Sens. Actuators, A **A91**, 2 (2001).
[26] M. Shima, L. Salamanaca-Riba, R. McMicheal, and T. Moffat, J. Electrochem. Soc. **149**, C439 (2002).
[27] S. K. Ghosh, P. Choudhury, S. K. Gupta, G. Ravikumar, M. S. Kumar, D. K. Aswal, R. O. Dusane, and A. K. Grover, Appl. Phys. Lett. **89**, 132507 (2006).
[28] Q. X. Liu, L. Péter, J. Tóth, L. F. Kiss, A. Cziráki, and I. Bakonyi, J. Magn. Magn. Mater. **280**, 60 (2004).
[29] L. Péter, V. Weihnacht, J. Tóth, J. Pádár, L. Pogány, C. M. Schneider, and I. Bakonyi, J. Magn. Magn. Mater. **312**, 258 (2007).
[30] Q. X. Liu, L. Péter, J. Pádár, and I. Bakonyi, J. Electrochem. Soc. **152**, C316 (2005).
[31] I. Bakonyi, L. Péter, V. Weihnacht, J. Tóth, L. F. Kiss, and C. M. Schneider, J. Optoelectron. Adv. Mater. **7**, 2 (2005).
[32] N. Wiser, J. Magn. Magn. Mater. **159**, 119 (1996).
[33] B. J. Hickey, M. A. Howson, S. O. Musa, and N. Wiser, Phys. Rev. B **51**, 667 (1995).
[34] S. K. J. Lenczowski, C. Schönenberger, M. A. M. Gijs, and W. J. M. de Jonge, J. Magn. Magn. Mater. **148**, 455 (1995).
[35] JCPDF Database International Centre for Diffraction Data, PA, Card No. PDF/150806, PDF/0.040836, 1998.
[36] D. S. Lashmore and M. P. Dariel, J. Electrochem. Soc. **135**, 1218 (1988).
[37] M. Pedersen, I. Bnicke, E. Lgsgaard, I. Stensgaard, A. Ruban, J. K. Nrskov, and F. Besenbacher, Surf. Sci. **387**, 86 (1997).
[38] H. W. Chang, F. T. Yuan, Y. D. Yao, W. Y. Cheng, W. B. Su, C. S. Chang, C. W. Lee, and W. C. Cheng, J. Appl. Phys. **100**, 084304 (2006).
[39] M. Shima, L. Salamanaca-Riba, R. McMicheal, and T. Moffat, J. Electrochem. Soc. **148**, C518 (2001).
[40] D. J. Larson, A. K. Petford-Long, A. Cerezo, G. D. W. Smith, D. T. Foord, and T. C. Anthony, Appl. Phys. Lett. **73**, 1125 (1998).
[41] J. W. Cai, S. Okamoto, O. Kitakami, and Y. Shimada, Phys. Rev. B **63**, 104418 (2001).
[42] L. Neel, J. Phys. Radium **17**, 250 (1956).
[43] L. Péter, Z. Rolik, L. F. Kiss, J. Tóth, V. Weihnacht, C. M. Schneider, and I. Bakonyi, Phys. Rev. B **73**, 174410 (2006).
[44] J. O. Oti, S. E. Russek, S. C. Sanders, and R. W. Cross, IEEE Trans. Magn. **32**, 590 (1996).